OPTIMAL PLACEMENT OF POWER QUALITY MONITORS FOR ENHANCED OBSERVABILITY WITH FEWER DEVICES

Markus de Koster[12*], Patrick Lehnen[12], Patrick Mack[12] , Eberhard Waffenschmidt[12], Ingo Stadler[12], Ahmad Bkira[2]

[1]*Cologne Institute for Renewable Energy, Technische Hochschule Köln, Cologne, Germany*
[2]*Institute of Electrical Power Engineering, Technische Hochschule Köln, Cologne, Germany*
**markus.de_koster@th-koeln.de*

Keywords: POWER QUALITY MONITORING, MEASUREMENT PLACEMENT, SPECTRAL CLUSTERING, SINGULAR VALUE DECOMPOSITION

Abstract

This paper presents a power quality monitor placement method that balances observability with minimal measurement devices. The approach constructs an affinity matrix capturing how transients, harmonics, and voltage sags propagate through the network. By aggregating voltage and current data under varying thresholds, a scree-plot analysis using singular value decomposition identifies the optimal number of monitors. Tests on multiple grids demonstrate that only a few power quality monitors can capture the dominant variance. Experimental results confirm improved harmonic state estimation when voltage monitors are placed at nodes far from strong voltage sources and on less supported feeders and the opposite for current monitors. This method considers various disturbance types, downstream tasks and scales more efficiently than existing methods.

1 Introduction

Monitoring of power quality in distribution grids is gaining importance with the increase of distributed inverter-based generation and significant non-linear loads. Power quality disturbances can lead to premature aging of components and equipment failure. These events often go unnoticed by distribution system operators (DSOs) due to insufficient power quality (PQ) monitoring.

Placing power quality monitors (PQM) in low-voltage grids faces multiple constraints. Many grid sections are underground, limiting where PQM can be installed. Diverse energy production and consumption patterns exacerbate the challenge. Furthermore, disturbances affect not only their node of origin but also spread throughout adjacent grid sections. Real-time data retrieval and synchronization are crucial for DSOs to correctly assess grid conditions.

1.1 Literature Review

Numerous studies have addressed the problem of optimally placing measurement devices in power systems. Only few address power quality disturbances in distribution networks and even fewer consider adaptability to downstream tasks as objective.

The authors of [1] define a monitor reach area as the region where at least one monitor detects a fault. A binary coverage matrix is constructed using measurement and error nodes, where entries indicate if the residual fundamental voltage at a node falls below a threshold. The approach is limited to voltage sags from short circuits and is formulated as an optimization problem. A topological graph theory approach achieving full observability is presented in [2]. The authors build a spanning measurement tree of full rank placing a total of 18 phasor measurement units in the IEEE 57-bus grid. Other methods focus on placing measurements in a way that optimizes the results of a state estimation. In [3] a cost-benefit analysis is combined with a power flow estimation to reduce the overall costs, selecting 10 measurement locations in a 99-node grid. The authors of [4] and [5] use a genetic algorithm as a metaheuristic approach to approximate the optimal locations verified through a weighted least squares state estimation (SE). In [6] a seeker optimization is combined with a harmonic state estimation (HSE) to find the optimal PQM placement in the IEEE 14-bus grid with 4 fixed harmonic sources achieving full observability with 7 PQM.

Overall, the optimization functions are computationally expensive and algorithms that aim at achieving full observability require significant amounts of PQM. Thus, data-based methods are on the rise that find good approximations of the system state even with few PQM[7], [8], [9]. Furthermore, with few exceptions ([6], [10]) most algorithms focus either only on power flow or consider only voltage sags as PQ disturbance.

2 Methodology

A use-case–oriented algorithm is proposed for selecting measurement locations in power distribution grids. Full observability through conventional SE requires a large number of measurement devices, but simpler cases like fault detection or SE using machine learning algorithms may only require small residuals to be captured. The algorithm must therefore adapt to diverse requirements while scaling efficiently to larger networks.

2.1 Simulating Power Quality Disturbances

In total, three grids were selected as test scenarios for the placement algorithm:

A) CIGRE low voltage distribution grid [11]
B) 14 node laboratory microgrid
C) IEEE 33-bus medium voltage (MV) grid [12]

Each of those grids was modelled in OpenDSS.

Then, two types of disturbances were simulated: a transient and a voltage sag. Each node in each of the grids was subjected to each fault once with PQM located at all nodes capturing the residuals of the fault.

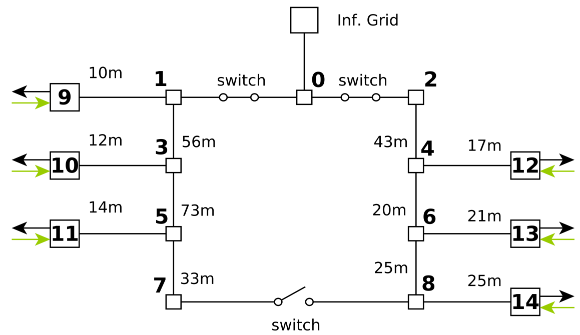

Figure 1: Microgrid with 6 controllable inverters (node 9-14) causing significant harmonic distortions.

2.2 Affinity Matrix

An affinity matrix (AM) was constructed to quantify how strongly a disturbance at node *d* is "seen" by a measurement device at node *m*. For a single frequency, the affinity entry $AM_{d,m}$ is defined as:

$$AM_{d,m} = |(v_{m,i} - v_{m,e})| / |(v_{d,i} - v_{d,e})|$$

where

- $v_{m,i}$ is the measured voltage phasor at node m during the disturbance
- $v_{m,e}$ is the measured voltage phasor at node m in the pre-disturbance condition
- $v_{d,i}, v_{d,e}$ are the analogous voltages at the disturbance node d.

The ratio $AM_{d,m}$ lies within [0,1], where 0 indicates that the disturbance at *d* has no effect on *m*, and 1 indicates that node *m* experiences the same relative voltage deviation. For current-based measurements, an analogous definition is used with current phasors. This formulation is then extended to multiple frequencies *f* by stacking additional AM layers or dimensions.

2.2.1 Aggregation: Using this affinity matrix, it is possible to analyse the spread of a PQ disturbance from one node to another. However, an algorithm that finds the optimal measurement location across multiple types of disturbances and for each frequency needs to consider all at once. Therefore, the different types of disturbances were aggregated as follows: If a frequency component appears in only one disturbance type, the original value is used. When two or more disturbances share the same frequency, the values of the AM are equal since the impedance that influences the error spread is equal. When merging frequency components, the mean across all frequency channels is calculated to produce a single aggregated matrix. Other strategies, such as minimum or weighted averaging, can be adopted in worst-case-scenarios or if certain harmonics are more critical for the use case.

Additionally, two monitoring scenarios are considered: Voltage-only measurements (I.) and combined voltage and current measurements (II.)

For the combined approach, a max aggregation is proposed: $AM_{d,m}^{combined} = max(AM_{d,m}^{voltage}, AM_{d,m}^{current})$

This choice ensures that if either current or voltage reveals a given disturbance more strongly, the aggregated AM captures that information. Depending on the use case, this strategy can be adapted to mean aggregation or to include weights e.g. in case monitoring of voltage characteristics is required due to sensitive equipment.

2.2.2 Thresholds: Two thresholds modulate how the AM values translate to recognizing disturbances:

- Minimum Threshold *min_threshold*. All AM values below this threshold are set to zero. This filters out minor deviations and noise.
- Maximum Threshold *max_threshold*. All AM values above this threshold are set to one. This identifies situations where a disturbance is "sufficiently recognized" for the given application.

These thresholds enable tuning for different use cases and for desired accuracy of downstream tasks like state estimation.

2.2.3 Asymmetry: Because the Thevenin-equivalent impedance Z_{th} seen by each disturbance node differs significantly, the matrix is generally not symmetric. This asymmetry reflects the reality that a strong source will drive a higher short-circuit current toward the fault location. Since $AM_{d,m} \neq AM_{m,d}$ in general, the matrix can be interpreted as a directed graph in graph-theoretical terms. Classical approaches that assume symmetric relationships (e.g., covariance-based methods) are not directly applicable. Thus, standard methods like principal component analysis (PCA), which require symmetric input matrices, may be unsuitable without modification.

2.3 Main Algorithm

A brute-force approach would evaluate all possible combinations of measurement nodes for a given number of devices. This is computationally intensive – particularly for larger networks – because the number of node subsets grows exponentially. Instead, the proposed method leverages spectral analysis techniques:

1. **Compute the aggregated AM**: Combine results across different disturbances and frequencies as

described and as deemed useful for the specific use case, applying min-max thresholds if desired.

2. **Perform Eigenvalue or Singular Value Decomposition (EVD / SVD)**: On the row-normalized AM, EVD is performed to find the eigenvalues and eigenvectors. This step is explained in more detail below.
3. **Determine Clusters and significant nodes**: Low or zero-valued eigenvalues often point to redundant measurement information, whereas large singular values correspond to dominant disturbance patterns. Techniques such as k-means clustering can identify nodes with similar affinity profiles.
4. **Select Monitor Nodes**: For each cluster, choose one node that exhibits maximal coverage (i.e., highest aggregated AM) to ensure that disturbances are adequately observed.

The directed spectral clustering approach starts by forming a row-stochastic transition matrix *P* from the non-negative affinity matrix AM so that each row of *P* sums to 1:

$$P_{i,j}=AM_{d,m}/(\sum_j of\ AM_{d,m})$$

To find the left eigenvectors of *P*, the right eigenvectors of the tranposed matrix P^T are computed $P^T v=\lambda v$ with *v* as the eigenvector and λ as the corresponding eigenvalue.
The eigenvalues λ are then sorted in descending order based on their real part. Note that at this step the eigenvalues may be complex numbers since the matrix is asymmetric.
Then, the eigenvectors corresponding to the top *n* components are selected where *n* is a parameter of the algorithm. In the process $n=2$ was found to be a good value to receive meaningful clusters. [13] Those top *n* eigenvectors form an embedding matrix *E* which is then normalized and clustered via *k-means.*This procedure identifies *k* groups of nodes that exhibit similar "directional" relationships in the directed graph defined by the affinity matrix. The computational complexity for typical implementations of SVD or EVD on an n×n matrix is on the order of $O(n^3)$, significantly smaller than the runtime for combinatorial optimization $O(2^n)$ for grids larger than $n=10$ nodes.

2.4 Restrictions and further applications

The algorithm assumes that each PQ meter provides time-synchronized measurements (e.g., via GPS). A similar procedure can be adapted for power-flow–related metrics. Instead of quantifying how strongly a fault at node *d* manifests at node m, the AM could represent the impact of a power injection on local voltage drops.
Gaussian measurement noise is handled by setting the *min_threshold* higher than the expected standard deviation. More complex, systematic sensor errors may require additional steps or extra monitor installations for redundancy.
Since the Thevenin-equivalent impedance is highly dependent on the source characteristic, the algorithm relies on an accurate description of the grid. Moreover, Thevinin impedance of solar systems changes with level of irridation. With the increase of distributed generation the upstream grid section may no longer exhibit the lowest equivalent impedance.

3 Results

3.1 Finding the optimal amount of measurements

First, the required amount of measurement devices is estimated. For this, we calculate the explained variance ratio *evr* of the 10 most significant singular values based on the formula $evr_i=\sigma_i^2(\sum_{k=1}^{r}\sigma_k^2)^{-1}$ with *r* as the rank of the data matrix and σ_i as the *i*-th singular value of the centered data matrix. Here, the denominator represents the total variance present in the data after centering. The procedure is repeated for selected sets of min-max thresholds and plotted for the voltage and current AM individually in a scree plot in figure 2.

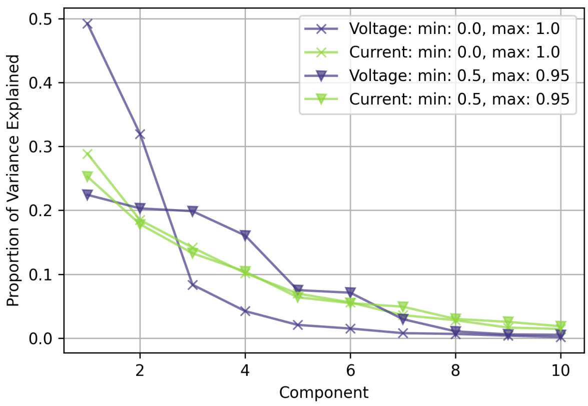

Figure 2: Scree plot of the explained variance ratio found through singular value decomposition of the affinity matrix. The y-axis shows the proportion of variance explained by the respective component (i.e. measurement device, on x-axis)

Typically, selecting the number of components corresponding to the "knee" of the scree plot curve is a reasonable choice. For voltage monitoring, using 3 to 4 measurement devices provides a balanced solution. However, with a high minimum threshold of 0.5, additional measurement devices are required. This approach may be particularly advantageous for use cases that demand the capture of significant residuals or in grids where measurement devices are expected to have high noise levels.
Since most PQM are capable of measuring voltage and current, we combine the affinity matrices through mean aggregation and show the scree plot in figure 3. The scree plot illustrates how the choice of thresholds

affects the proportion of variance explained by each component. A lower max threshold leads to the first component capturing a larger share of the total variance, reflecting the idea that errors are more broadly captured by the leading component.

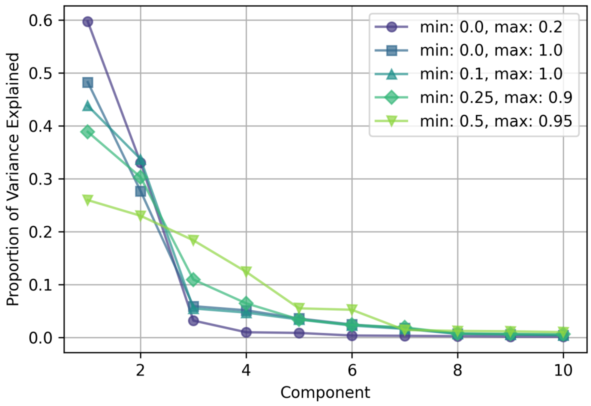

Figure 3: Scree plot for combined current and voltage measurements for different thresholds.

In contrast, a higher min threshold results in a flatter curve, as the variance becomes more evenly distributed across components. In this case, the largest eigenvalues no longer effectively capture specific errors, as the stricter threshold filters out smaller contributions, requiring additional components to represent the variance adequately.

3.2 CIGRE low voltage grid

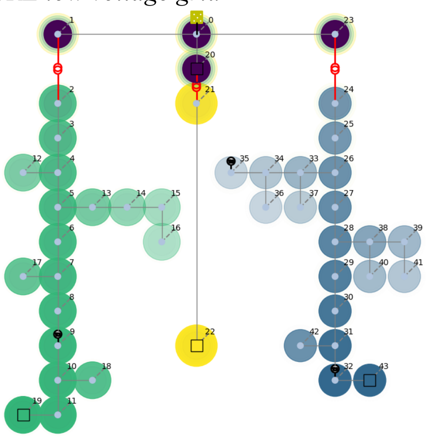

Figure 4: Optimal placement of 4 PQM (colored squares) considering voltages for various frequencies. Opacity of circles shows percentage of error captured by the respectively colored measurement node.

For the CIGRE low voltage distribution grid, optimal placement of 4 voltage-only measurement devices is determined by first clustering the grid into 4 sections and then selecting optimal PQM locations within each cluster. As shown in figure 4, three devices are placed in the LV section at the end of long feeders away from the upstream grid, and one PQM in the MV section.

Here, the transparency of each circle around the node shows the aggregated percentage of the total residual arriving at the respectively colored measurement location. Fully transparent circles show that no residual remains while opaque circles signify a majority of residual was captured by the measurement device.

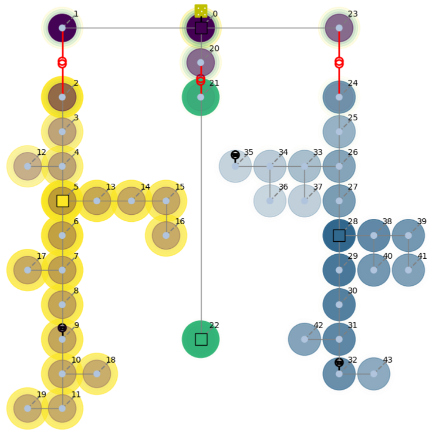

Figure 5: Optimal placement of 4 PQM considering voltages and currents aggregated through mean values. Measurements are placed at central junctions and in the industrial section at the distanced node.

When combining current and voltage through mean aggregation, the measurement devices are placed in central locations of the feeders as shown in figure 5.

3.3 Microgrid

For the microgrid, two voltage-monitoring PQM were selected based on the evr calculation and placed at nodes 11 and 14.

To validate the placement further, two HSE models were employed to estimate the state of the first 25 harmonic voltages. The HSE concept is based on the work in [9]. Both models utilized fully connected neural networks, with harmonic voltages measured at two PQMs as inputs and harmonic voltages at all nodes as outputs. Verification was performed using real data collected by PQMs installed at 10 out of the 14 nodes, and the results are presented below. The neural networks were trained with two hidden layers, each containing 750 neurons, over 1000 epochs. No additional hyperparameter tuning was performed.

With monitors placed optimally at nodes 11 and 14, the Mean Absolute Error (MAE) is 0.0215, which is lower than the MAE of 0.0246 observed under suboptimal placement at nodes 6 and 9. This shows that with optimal PQM placement, the HSE is more accurate than with suboptimal placement.

For the combination of voltage and current monitoring, two PQM were selected and placed at central junctions (node 3 and 4).

3.4 IEEE 33-bus

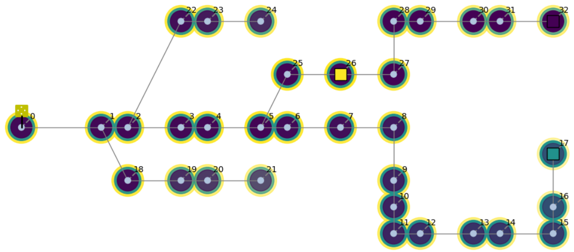

Figure 6: In the IEEE 33-bus grid, errors propagate more significantly and residuals are captured well even at distanced nodes.

When monitoring only the voltage, 3 PQM were placed at nodes 17, 26 and 32 in the IEEE 33-bus grid as shown in figure 6. Through mean aggregation of voltage and current the locations 3, 18 and 25 were identified as optimal.

4 Conclusion

A data-driven monitor-placement algorithm was introduced, using an affinity matrix to capture how various PQ disturbances propagate through distribution grids. By thresholding and aggregating voltage/current measurements, the method applies spectral decomposition to estimate the required number of PQ monitors without relying on combinatorial searches or iterative optimization, enabling efficient scalability to larger networks.

For practical deployment, the method yields clear recommendations: voltage monitors should be placed away from strong sources to maximize disturbance visibility. Current-measuring PQMs are most effective when placed at feeder origins while combined voltage and current sensors are best located at key network junctions. These recommendations for DSOs are generalizable to different grid topologies, if approximate grid information is available.

Validation through HSE based on neural networks on multiple test networks confirmed that the selected monitor locations yield improved accuracy compared to suboptimal placements. The algorithm's moderate runtime and capacity to handle both voltage and current measurements make it readily applicable for real-world applications. Overall, this methodology enables DSOs to deploy fewer PQ monitors while capturing a broad spectrum of disturbances, thus optimizing both installation cost and observability.

5 Acknowledgements

This research was funded by the German Federal Ministry for Economic Affairs and Climate Action grant number 03EI4048R.

6 References

[1] V. Ferreira, et al, "Optimal location of Power Quality Monitors in distribution grids based on MRA methodology," *REPQJ*, vol. 20, pp. 24–29, Sep. 2022

[2] N. Xie, F. Torelli, E. Bompard et al., "A graph theory based methodology for optimal PMUs placement and multiarea power system state estimation," *Electric Power Systems Research*, vol. 119, pp. 25–33, Feb. 2015

[3] M. Pau, M. Ginocchi, D. Pacheco et al., "A Meter Placement Strategy for Distribution Grids Based on Cost–Benefit Analysis," *IEEE Transactions on Instrumentation and Measurement*, vol. 73, pp. 1–12, 2024

[4] M. Cramer, P. Goergens, F. Potratzet al., "Genetic Algorithm for Optimal Meter Placement and Selection in Distribution Grid State Estimation," in *International ETG Congress 2015*, Nov. 2015, pp. 1–7.

[5] S. Hubschneider, M. Uhrig, M. Suriyahet al., "Optimized meter placement in low voltage grids based on asymmetric state estimation," in *52nd International Universities Power Engineering Conference (UPEC)*, Aug. 2017, pp. 1–6.

[6] A. Ketabi, M. R. Sheibani, and S. M. Nosratabadi, "Power quality meters placement using seeker optimization algorithm for harmonic state estimation," *International Journal of Electrical Power & Energy Systems*, vol. 43, no. 1, pp. 141–149, Dec. 2012

[7] M.-Q. Tran, A. S. Zamzam, P. H. Nguyen et al., "Multi-Area Distribution System State Estimation Using Decentralized Physics-Aware Neural Networks," *Energies*, vol. 14, no. 11, Jan. 2021

[8] O. Kundacina, G. Gojic, M. Cosovic et al., "Scalability and Sample Efficiency Analysis of Graph Neural Networks for Power System State Estimation," Mar. 02, 2023.

[9] P. Mack, M. de Koster, P. Lehnen et al., "Power Quality State Estimation for Distribution Grids Based on Physics-Aware Neural Networks—Harmonic State Estimation," *Energies*, vol. 17, no. 21, Art. no. 21, Jan. 2024

[10] S. Ali, K. Wu, K. Weston et al., "A Machine Learning Approach to Meter Placement for Power Quality Estimation in Smart Grid," *IEEE Transactions on Smart Grid*, vol. 7, no. 3, pp. 1552–1561, May 2016

[11] Conseil international des grands réseaux électriques, Ed., *Benchmark systems for network integration of renewable and distributed energy resources*. Paris: CIGRÉ, 2014.

[12] M. E. Baran and F. F. Wu, "Network reconfiguration in distribution systems for loss reduction and load balancing," *IEEE Transactions on Power Delivery*, vol. 4, no. 2, pp. 1401–1407, Apr. 1989

[13] H. Sevi, M. Jonckheere, and A. Kalogeratos, "Generalized Spectral Clustering for Directed and Undirected Graphs," Mar. 14, 2022